AD-A032 756 CALIFORNIA UNIV LIVERMORE LAWRENCE LIVERMORE LAB F/G 11/6
BEHAVIOR OF POROUS BERYLLIUM UNDER THERMOMECHANICAL LOADING. PA--ETC(U)
OCT 74 R N SCHOCK, A E ABEY, A G DUBA W-7405-ENG-48

UNCLASSIFIED UCRL-51682-PT-2 NL

1 OF 1
AD A032756

END

DATE FILMED
2-77

UCRL-51682 Pt. 2

BEHAVIOR OF POROUS BERYLLIUM UNDER THERMOMECHANICAL LOADING: PART 2. QUASI-STATIC DEFORMATION

R. N. Schock
A. E. Abey
A. G. Duba

October 16, 1974

Prepared for U.S. Atomic Energy Commission under contract No. W-7405-Eng-48

LAWRENCE LIVERMORE LABORATORY
University of California/Livermore

Printed in the United States of America
Available from
National Technical Information Service
U.S. Department of Commerce
5285 Port Royal Road
Springfield, Virginia 22151
Price: Printed Copy $___*; Microfiche $2.25

*Pages	NTIS Selling Price
1-50	$4.00
51-150	$5.45
151-325	$7.60
326-500	$10.60
501-1000	$13.60

TID-4500, UC-34
Physics-General

LAWRENCE LIVERMORE LABORATORY
University of California/Livermore, California/94550

UCRL-51682-Pt-2

BEHAVIOR OF POROUS BERYLLIUM UNDER THERMOMECHANICAL LOADING. PART 2. QUASI-STATIC DEFORMATION

R. N. Schock
A. E. Abey
A. G. Duba

MS. date: October 16, 1974

16 Oct 74

20p.

W-7405-Eng-48

390 999 LB

Preface

This report is Part 2 of a seven-part series on Behavior of Porous Beryllium Under Thermomechanical Loading (UCRL-51682 Pts. 1-7). The titles and authors of the individual reports in the series are as follows:

Title	Authors
Part 1. Summary of Results	W. M. Isbell
Part 2. Quasi-Static Deformation	R. N. Schock, A. E. Abey and A. G. Duba
Part 3. Shock Wave Studies	W. M. Isbell, R. R. Horning
Part 4. Constitutive Model for Wave Propagation	F. H. Ree, W. M. Isbell, and R. R. Horning
Part 5. Electron-Beam Studies	O. R. Walton, W. M. Isbell
Part 6. Effect of Pressure on the Microstructure of Plasma-Sprayed Beryllium	J. E. Hanafee, E. O. Snell
Part 7. Calibration Studies on the Carbon Piezoresistive Gage	R. R. Horning, W. M. Isbell

This work was supported by the Defense Nuclear Agency (Mr. Donald Kohler, technical monitor) under the auspices of the U.S. Atomic Energy Commission.

Contents

BEHAVIOR OF POROUS BERYLLIUM UNDER THERMOMECHANICAL LOADING: PART 2. QUASI-STATIC DEFORMATION

Abstract

Loading and unloading of two types of porous beryllium under conditions of uniaxial strain and hydrostatic pressure indicate that the total volume change before the onset of yielding is small and that there is a maximum stress-porosity function which describes pore-collapse, independent of loading and unloading cycles. Comparison of the data taken prior to yielding with theoretical models shows the influence of aspherical pores which result in increased compressibility on initial loading. Initial yielding is much more distinct in the sintered than in the unsintered material and is believed to be an indication of the presence of pores of higher average sphericity produced by the sintering process. Both materials exhibit shear-enhanced compaction when loaded in uniaxial strain.

Introduction

In this report we present deformation measurements on both unsintered and sintered, plasma-sprayed, porous beryllium. We have performed two types of experiments: loading and unloading under conditions of uniaxial strain and of hydrostatic pressure. In uniaxial strain loading, an axial stress is applied to a cylindrical sample with the condition that radial strain remain constant. This is achieved by control of the confining pressure and results in a loading path that duplicates that path thought to represent plane shock-loading. However, deformation is at much lower strain rates. The results of these experiments will be compared with data from shock-wave experiments and interpreted in terms of the possible deformation models.

The experimental techniques used in these studies have been described previously.[1,2] The starting material[3] consisted of plane disks (19 mm in diameter × 4.6 mm) which were coated with a semi-flexible epoxy and fitted with foil-strain gages to measure circumferential and axial strain. They were then exposed to hydrostatic pressures of up to 0.8 GPa in determining the pressure-volume relationship. For higher pressures (to 4.0 GPa), tin was used as a pressure medium (quasi-hydrostatic). In this case it was necessary to fabricate a sample about 25 mm in height and 11 mm in diameter by stacking of disks. This technique was also used in fabricating samples for use in uniaxial-strain measurements where strain gages were applied to the center disk. In this case,

end plugs which serve as force-applying pistons are cemented to the top and bottom of the stacked disks while they are coated with epoxy. The average density, determined by measuring and weighing each disk was found to be 1.587 ± 0.004 Mg/m^3 for the unsintered material and 1.647 ± 0.006 Mg/m^3 for the sintered material. This corresponds to porosities of 14.2 and 11.0%, respectively.

Experimental Results

PRESSURE-VOLUME

The pressure-volume relationship for unsintered beryllium is shown in Fig. 1. Two sets of data are shown, one for the quasi-hydrostatic results and a second for the hydrostatic. The unloading results shown in Fig. 1 are actual data for the entire hydrostatic portion and for only the lower two-thirds of the quasi-hydrostatic curves. The remaining portions of the quasi-hydrostatic curves are extrapolations. The rather large differences between the two sets of data (hydrostatic and quasi-hydrostatic) could result from one or more of a number of possible causes. One of these may be the difference in stress state between hydrostatic and quasi-hydrostatic tests. In this case, the two sets of data would agree above some pressure where the effect of the shear stress in the quasi-hydrostatic test becomes unimportant. The dashed line shown in Fig. 1 is our estimate of how these two sets of data would merge.

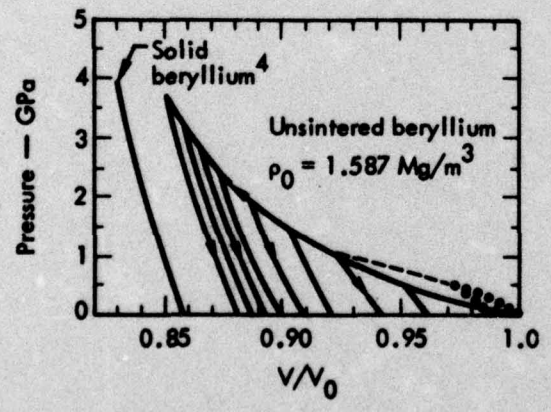

Fig. 1. Pressure-volume relationship for unsintered beryllium. Curve for solid beryllium shown for comparison. Points represent hydrostatic data and solid lines quasi-hydrostatic data. Dashed line is extrapolation of hydrostatic data.

A second possible cause of the discrepancy is that the stacking of disks could induce extra volume in the quasi-hydrostatic case even though great care was used in fabricating the disks. In addition, because the hydrostatic sample was smaller, it had a smaller volume-to-surface ratio than the quasi-hydrostatic sample. Then, when the hydrostatic sample was coated with epoxy, this could result in a reduction of the total porosity volume in comparison with the quasi-hydrostatic sample. With only one test for the hydrostatic measurements and only one test for the quasi-hydrostatic, it is not possible to unequivocally determine the cause of this difference. At the highest pressure (4 GPa), the material still has some porosity as exhibited by comparing the curve for porous beryllium with the curve for solid beryllium[4] shown at left in Fig. 1, and by noting that the unloading curve is steeper than the loading curve.

There is approximately 2.4% porosity which is not removed at 4.0 GPa. The unloading curves become steeper as the peak pressure increases.

The pressure-volume relationship for the sintered beryllium is shown in Fig. 2. In this case, hydrostatic data were taken to 0.8 GPa. As before only the lower two-thirds of the quasi-static unloading curves represent actual experimental data. Unlike the unsintered material, the sintered porous beryllium exhibits a pronounced yield* at about 0.4 GPa, where substantial pore crush-up presumably begins. Beyond this point, the slope decreases and begins to increase again only above 1.0 GPa. At 4 GPa there is, as with the unsintered material, some porosity remaining (about 2.2%). It should be noted again that there is a difference between the slopes of the loading and unloading curves, indicating that some porosity does still exist. The initial unloading slopes in Fig. 2 do not differ to the extent that they do in unsintered beryllium.

We feel that the discrepancy between the hydrostatic and quasi-hydrostatic results is best explained by the difference in stress state. This explanation is consistent with the Hugoniot[3] and with the porosity left in the samples after pressurization to 4 GPa as determined by Hanafee and Snell.[5] The unloading slopes for both materials from 4 GPa are, within experimental error, the same as the unloading slopes for solid beryllium.

*In this report we use the [illegible] "yield" in a broad sense to describe a pronounced change in the slope of a stress-strain curve.

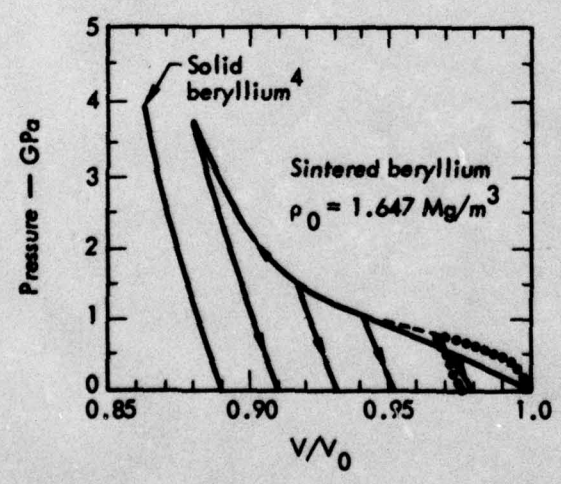

Fig. 2. Pressure-volume relationship for sintered beryllium. Curve for solid beryllium shown for comparison. Points represent hydrostatic data and solid lines quasi-hydrostatic data. Dashed line is extrapolation of hydrostatic data.

UNIAXIAL STRAIN

A sample of unsintered beryllium was also loaded and cycled under conditions of uniaxial strain along the differential stress-confining pressure paths shown in Fig. 3. On unloading, the differential stress ($\sigma_1 - \sigma_3$) falls off faster than the confining pressure ($\sigma_3 = \sigma_2$) in all cases. In some cases, only the differential stress was removed before reloading, while in others the confining pressure was also removed after the differential stress was removed, at which time the strain gages were usually replaced. In the cases where only the differential stress and not the confining pressure has been removed, the differential stress on reloading appears to rise to the same maximum stress level, at the same confining pressure, that was attained on the previous cycle. However, when reloading takes place from atmospheric

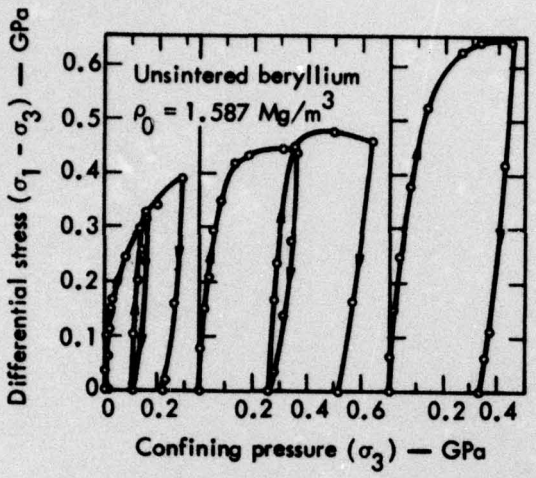

Fig. 3. Differential stress as a function of confining pressure for unsintered beryllium during uniaxial strain loading and unloading.

pressure, the axial differential stress approaches higher values at correspondingly lower confining pressure.

In Fig. 4 the axial stress is plotted against volume strain for the data corresponding to Fig. 3. In general, the maximum stress obtained on reloading is controlled by the requirement that, for a given specific volume, there is a stress (σ_1) which cannot be exceeded. Here, as with the pressure-volume data (Fig. 1), we observe no distinct yield stress upon initial loading. When the material is unloaded completely (to atmospheric confining pressure), a pronounced recovery of strain is observed at the lowest pressures. The compressional wave speed

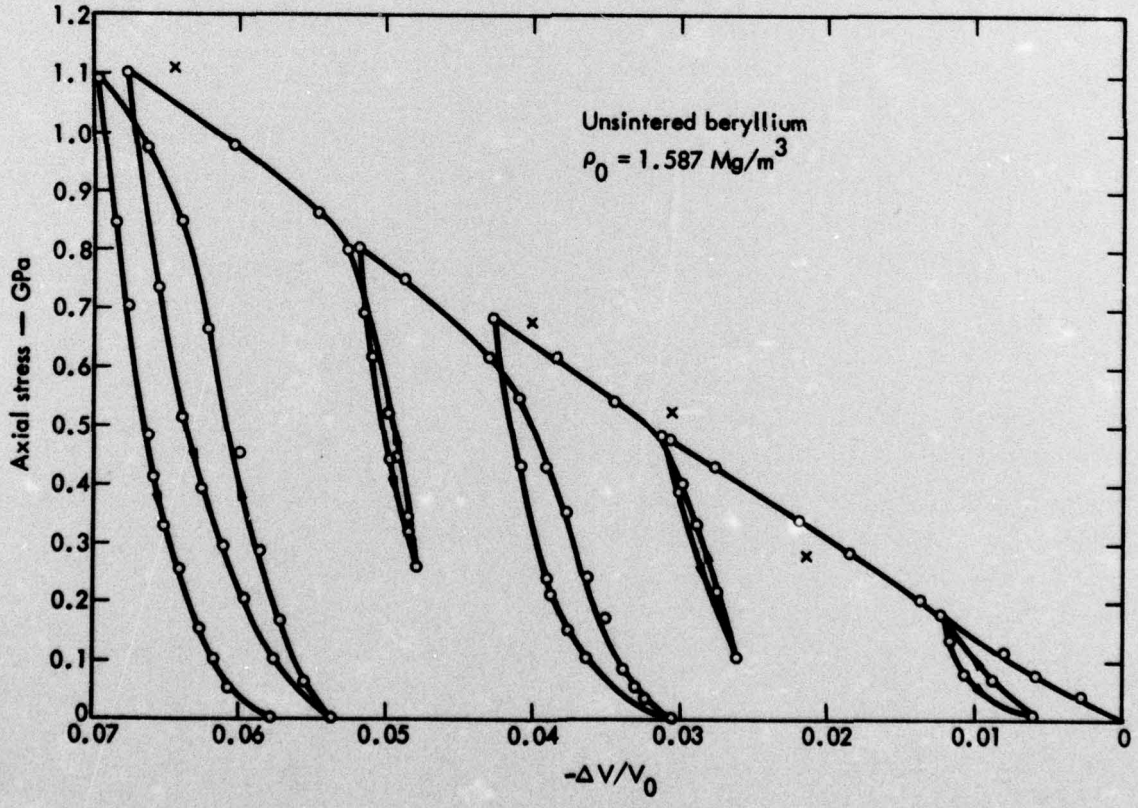

Fig. 4. Axial stress as a function of strain for unsintered beryllium during uniaxial strain loading and unloading. (x) represent shock-wave data points determined by Isbell and Horning.[3]

calculated from the initial loading slope in Fig. 4, assuming elasticity, is 3.0 km/s. The velocities obtained from the initial unloading slopes are given in Table 1. These velocities increase with axial stress and compression. With 7% of the porosity removed, the calculated value of 12.3 km/s is very close to the elastic wave speed at atmospheric pressure in fully dense beryllium of 12.89 km/s.[6]

Also shown in Fig. 4 are four data points determined at high strain rates (shock-wave) by Isbell and Horning.[3] Within experimental error, the points are coincident with the path that defines the maximum stress-volume strain curve.

The mean stresses (unloading and reloading data excepted) associated with the data in Fig. 4 are plotted in Fig. 5 and compared with the hydrostatic pressure-volume curve from Fig. 1. It is apparent that the shear stress in the uniaxial strain experiment enhances compaction at a given mean pressure.

Table 1. Calculated sound speeds on unloading for unsintered beryllium (ρ_0 = 1.587 Mg/m^3).

1st cycle	
	ρ = 1.610 Mg/m^3
	C = 7.0 km/s
2nd cycle	
	ρ = 1.644 Mg/m^3
	C = 8.8 km/s
3rd cycle	
	ρ = 1.666 Mg/m^3
	C = 9.2 km/s
4th cycle	
	ρ = 1.684 Mg/m^3
	C = 10.1 km/s
5th cycle	
	ρ = 1.713 Mg/m^3
	C = 10.3 km/s
6th cycle	
	ρ = 1.716 Mg/m^3
	C = 12.3 km/s

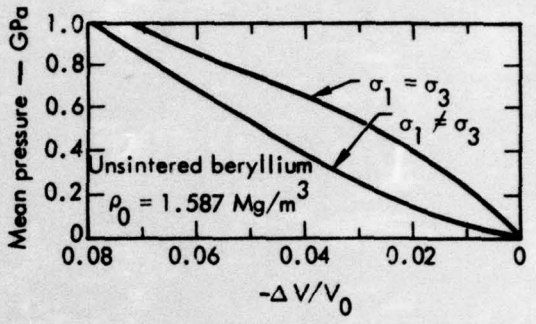

Fig. 5. Mean pressure as a function of volume strain for unsintered beryllium on uniaxial strain and hydrostatic loading (Fig. 1).

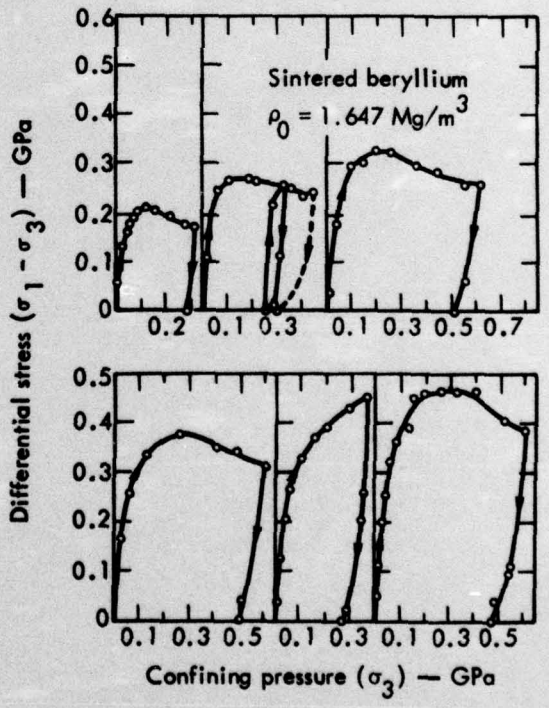

Fig. 6. Differential stress as a function of confining pressure for sintered beryllium during uniaxial strain loading and unloading.

The differential stress-confining pressure history of a sample of sintered porous beryllium loaded and unloaded in uniaxial strain is shown in Fig. 6. On one cycle, the sample was unloaded to zero differential stress only, on all others to atmospheric pressure. Again, the sample showed loading to higher axial stresses on successive reloading from the same confining pressure. However, in the sintered material there is a pronounced decrease in differential stress after the initial loading portion. This is a definite indication of an unstable process, since shear strain is accumulating while the shear stress is decreasing.

The axial stress-strain relationship is shown in Fig. 7 for the sintered beryllium. In contrast to the behavior in the unsintered material, a fairly distinct yield is observed between 0.1 and 0.3 GPa. This is similar to that observed for this material on hydrostatic loading. As before, we observe reloading to essentially the same stress and strain levels as attained before unloading. We also observe additional strain recovery on unloading at the lowest stress. The compressional velocity obtained from the initial loading slope of the data in Fig. 7 is 6.2 km/s. Calculated compressional wave speeds on unloading are shown in Table 2. In contrast to the unsintered material, the initial unloading slopes are almost constant for sintered material with between 1.4 and 4.9% of the porosity removed. All values are very close to the elastic wave speed in dense beryllium. Also plotted in

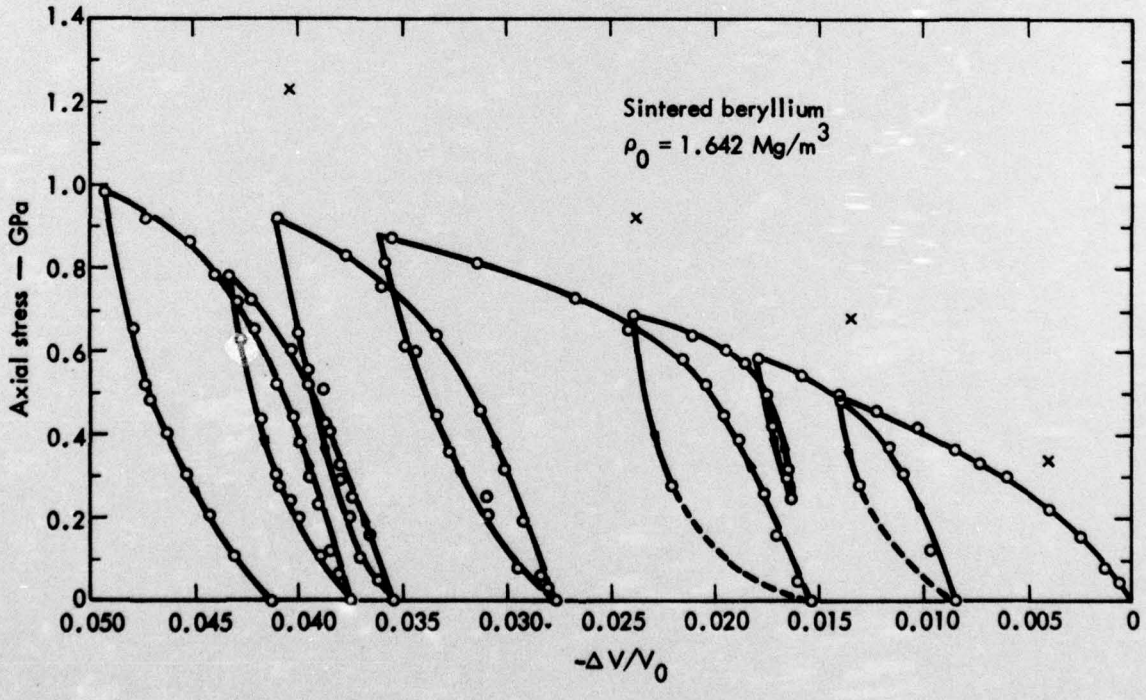

Fig. 7. Axial stress as a function of strain for sintered beryllium during uniaxial strain loading and unloading. (x) represent shock-wave data points determined by Isbell and Horning.[3]

Table 2. Calculated sound speed on unloading for sintered beryllium (ρ_0 = 1.647 Mg/m^3).

1st cycle	
	ρ = 1.672 Mg/m^3
	C = 12.2 km/s
2nd cycle	
	ρ = 1.680 Mg/m^3
	C = 11.98 km/s
3rd cycle	
	ρ = 1.691 Mg/m^3
	C = 10.1 km/s[a]
4th cycle	
	ρ = 1.713 Mg/m^3
	C = 11.2 km/s
5th cycle	
	ρ = 1.722 Mg/m^3
	C = 12.6 km/s
6th cycle	
	ρ = 1.726 Mg/m^3
	C = 12.3 km/s
7th cycle	
	ρ = 1.733 Mg/m^3
	C = 13.5 km/s

[a]Based on limited data.

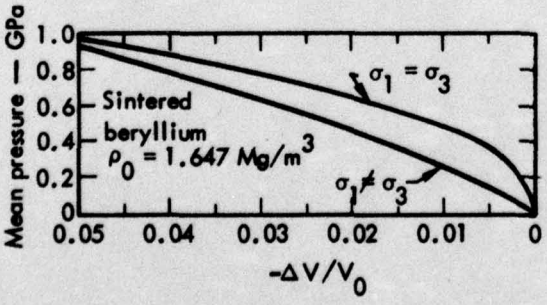

Fig. 8. Mean pressure as a function of volume strain for sintered beryllium on uniaxial strain and hydrostatic loading (Fig. 2).

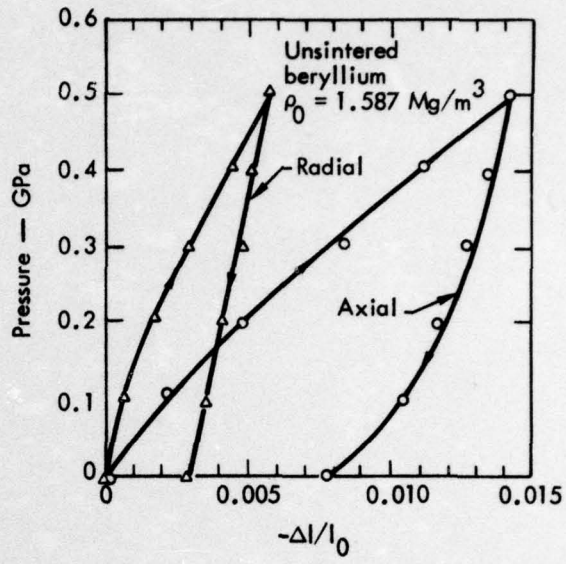

Fig. 9. Strain in radial and axial directions as a function of hydrostatic pressure for unsintered beryllium.

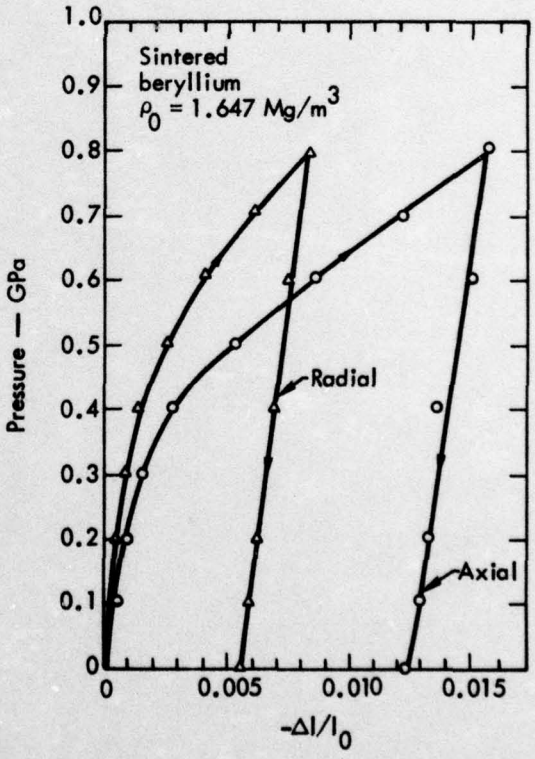

Fig. 10. Strain in radial and axial directions as a function of hydrostatic pressure for sintered beryllium.

Fig. 7 are shock-wave data obtained by Isbell and Horning.[3] These data lie consistently above the low strain-rate data.

The mean pressures associated with the axial stress data shown in Fig. 7 are plotted in Fig. 8 along with the hydrostat from Fig. 2. As with the unsintered material, the data in Fig. 8 indicate enhanced compaction in the presence of a macroscopic shear stress.

The axial and circumferential strain data taken on hydrostatic loading and unloading (Figs. 1 and 2) indicate that both materials compressed in an anisotropic manner. This is shown in Figs. 9 and 10 where the linear strain measured by both gages is shown on loading and unloading. The unsintered beryllium is more compressible in both directions than the sintered beryllium and both linear compressibilities contribute to the observed larger volume compressibility. The anisotropic data (Figs. 9 and 10) indicate that this effect is greater in the unsintered material where axial compressions exceed radial by almost 3:1; whereas in the sintered material the ratio is somewhat less than 2:1.

Discussion

Examination of the cyclic loading data in Figs. 4 and 7 indicate that 1) the total volume change before the onset of yielding is small compared to what takes place thereafter and 2) there appears to be a maximum stress-volume strain function, independent of loading and unloading cycles, which we interpret as yielding of the matrix. This suggests that the material may be loading up to a yield stress in a manner controlled primarily by the properties of the matrix and influenced by porosity only in a minor way. Porosity is lost in significant quantities only upon the attainment of a yield stress which is a function of porosity. These observations suggest two approaches to the development of constitutive relations to describe the behavior of these materials.

First, the loading up to the yield point may be considered in terms of a linearly elastic material, and second, pore-collapse may be treated in terms of theoretical models.

Such methods as the self-consistent approach of Mackensie[7] and later adaptations by Hashin[8] and Walsh et al.[9] are used to describe initial loading of porous materials. The loading to and from the measured yield surface (Figs. 4 and 7) is not entirely linear, but in terms of the overall equation-of-state this linearity seems to be a reasonable approximation. We might anticipate a deviation from these models due to the presence of aspherical holes produced in forming the material. This is suggested by the data in Fig. 11 where we show the effective bulk modulus, as a function of porosity η, determined from the initial unloading portions of the data on unsintered beryllium. We have chosen the initial unloading data because they are likely to best represent elastic behavior over a range of stresses. The theoretical relationship of Mackensie[7] is shown for comparison. We observe a lower effective bulk modulus which we attribute to the presence of aspherical

pores in the starting material. In a homogeneous stress field, aspherical pores are weaker than spherical pores. Thus the stiffness of the unsintered beryllium is less than for the same material with a regular array of spherical pores. At maximum compression, the data in Fig. 4 indicate about 7% porosity remaining. As is shown in Fig. 11, at this point the effective bulk modulus relationship converges with the value predicted using the theory of Mackensie. In principle this convergence should take place at zero porosity, and the sharp convergence with some porosity remaining may be the result of a nonuniform distribution of pore shapes. Thus at low pressures, most of the porosity removed would be highly aspherical, and the effective bulk modulus would be lower than that for the solid with only spherical pores. However, when most of this type of porosity has been removed, the effective bulk modulus will be higher and, based on the observed moduli in Fig. 11, the remaining porosity will behave as spherical or nearly spherical porosity. Some of the aspherical porosity is expected to be in the form of long narrow cracks and, upon the release of pressure, will re-open causing the volume to increase noticeably as observed in Fig. 4.

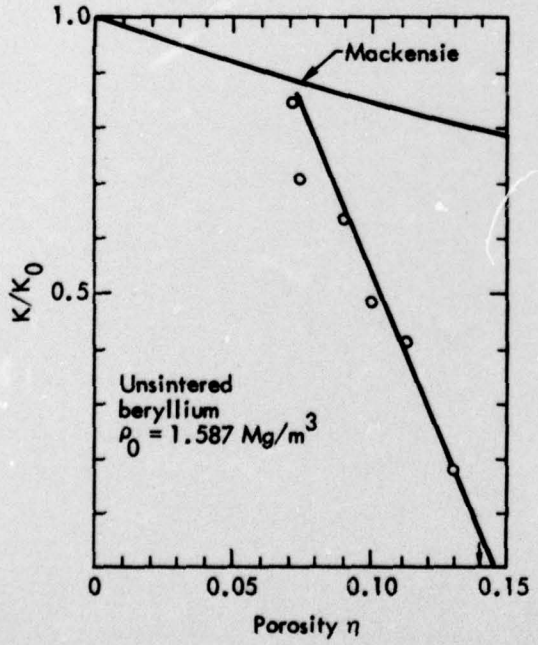

Fig. 11. Ratio of effective bulk modulus (K) for unsintered beryllium to bulk modulus of solid beryllium (K_0). Data are obtained from the initial unloading slopes in Fig. 4. Arrow represents initial porosity. Theoretical relationship of Mackensie[7] is shown for comparison.

In Figs. 12 and 13 we show photomicrographs[5] of unsintered and sintered beryllium starting material which afford a comparison of the pore geometry before and after sintering. Sintering reduces the total porosity at the expense of small pores. In addition, the highly irregular pore shapes present in the unsintered material have been changed into slightly more rounded spherical forms upon sintering.

In Fig. 14 we show the effective bulk modulus – porosity relationship for sintered beryllium determined from the initial unloading slopes in Fig. 7. The effective moduli are now much stiffer than for the unsintered material (compare the velocities obtained in Table 2 with those in Table 1). This means smaller strain values per unit stress and more percentage scatter in the effective moduli. The data in Fig. 14 cluster about Mackensie's theoretical prediction. Walsh et al.[9] have shown that Mackensie's prediction is also valid when the pores are slightly nonspherical. The data in Fig. 14 indicate that for the sintered material, Mackensie's model is

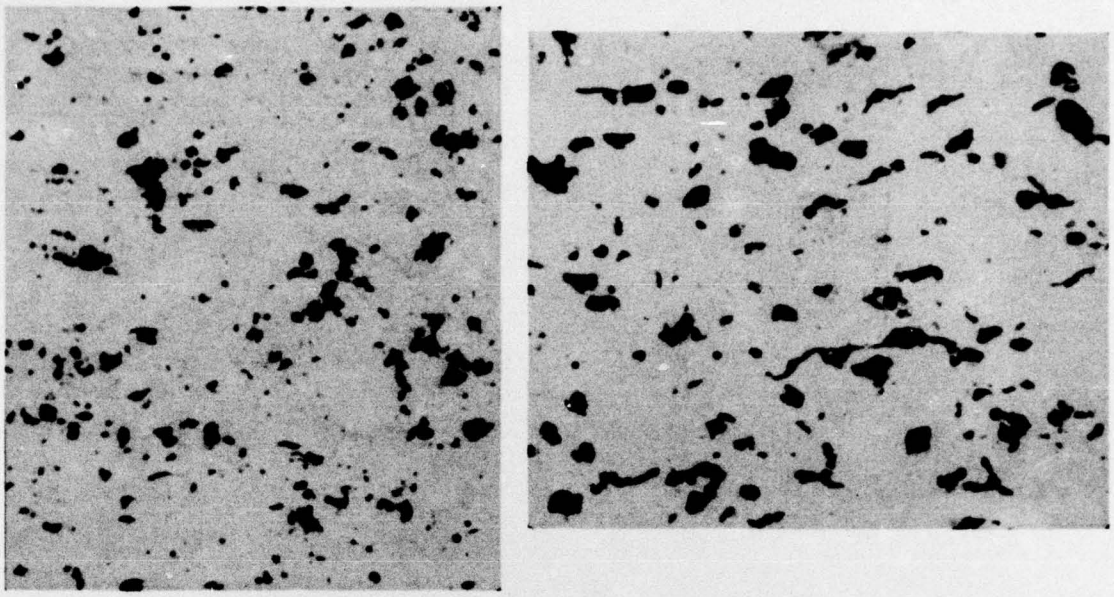

(a) (b)

Fig. 12. Photomicrographic comparison[5] of (a) unsintered and (b) sintered porous beryllium. Section is parallel to the direction of plasma spray (vertical). 400X.

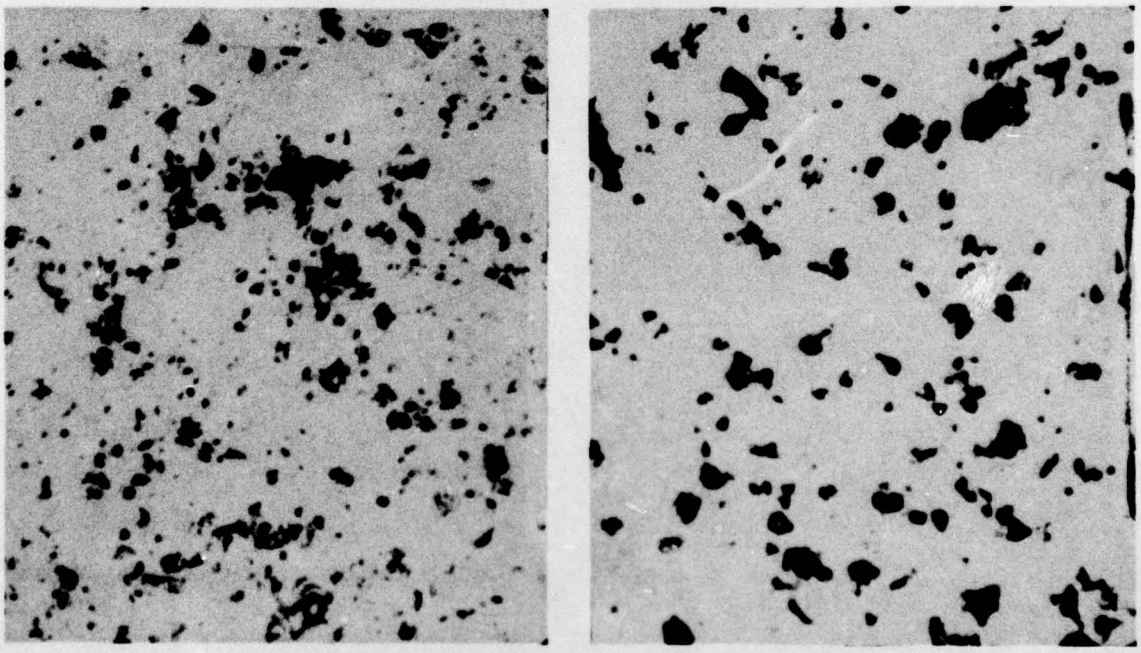

(a) (b)

Fig. 13. Photomicrographic comparison[5] of (a) unsintered and (b) sintered porous beryllium. Section is normal to the direction of plasma spray. 400X.

more closely followed than for the unsintered material. This is in agreement with the photomicrographic evidence in Figs. 12 and 13 that shows the sintered material having porosity which is more spherical.

Many models have been suggested to describe the behavior of porous solids as the porosity (η) is removed by the application of pressure (P). These are summarized by Heckel.[10] The most successful model appears to be that described by an equation of the form

$$P = a \ln (1/\eta) \qquad (1)$$

first used by Konopicky.[11] The proportionality constant a was shown by Heckel to be empirically related to the compressive yield strength (τ). In analysing the collapse of a hollow sphere, Carroll and Holt[12] showed that $a = 2/3\tau$, and that the onset of total plastic flow is controlled only by the value of τ.

The behavior of both sintered and unsintered beryllium in terms of Eq. (1) is shown in Fig. 15 where we have plotted the maximum stress data in Figs. 4 and 7 as a function of η. If the constitutive relation in Eq. (1) perfectly described the behavior in the pore collapse region, then the data in Fig. 15 would define a straight line. Above 0.1 GPa, the data for the unsintered beryllium essentially do this

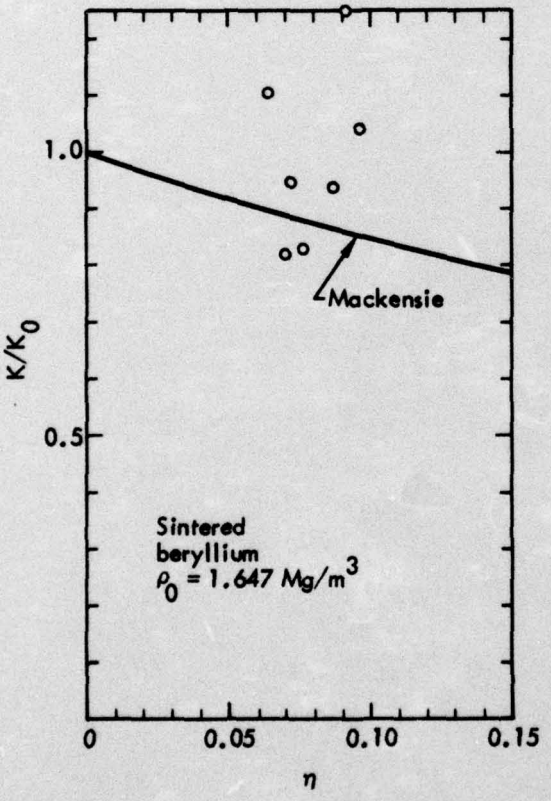

Fig. 14. Ratio of effective bulk modulus (K) for sintered beryllium to bulk modulus of solid beryllium (K_0). Data are obtained from the initial unloading slopes in Fig. 7. Arrow represents initial porosity. Theoretical relationship of Mackensie[7] is shown for comparison.

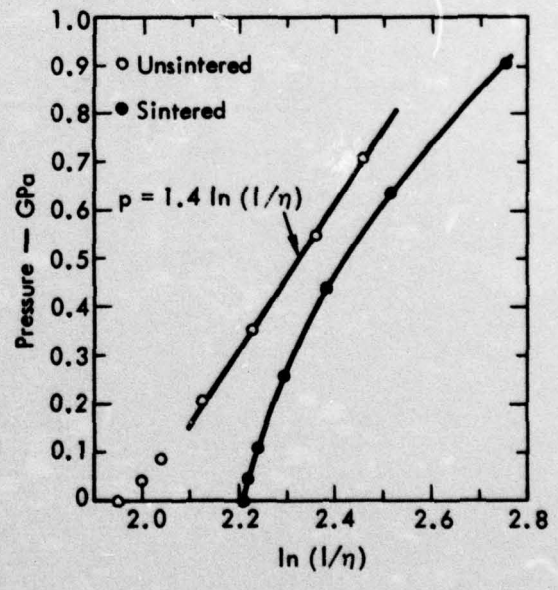

Fig. 15. Pressure as a function of ln (1/η) for porous beryllium from the data in Figs. 4 and 7.

with a slope of 1.4 GPa. However, below this pressure and for the sintered beryllium at all pressures, the data do not seem to fit this simple model. A simple interpretation of the data for the unsintered material indicates a very small yield, in agreement with previous observations. The data for the sintered material could be interpreted as the approach to a yield point above 0.9 GPa. If this behavior is indicative of what happens at high strain rates, then the material will not be able to support a stable shock wave in this stress region.

Since the data on uniaxial strain loading involve the presence of appreciable amounts of shear stress, a fairer test of the applicability of Eq. (1) may be made with the hydrostatic data in Figs. 1 and 2. This is done in Fig. 16. A reasonable approximation to a linear relationship may be made by fitting the data for unsintered beryllium to a line with a slope of about 2.0 GPa. The sintered beryllium data in Fig. 16 show a continuously decreasing slope over the same pressure range as in Fig. 15 but at higher pressures the slope reverses. The data for sintered beryllium in Fig. 16 above 0.6 GPa do not lie on a straight line. However, in comparison with the previous analysis for unsintered beryllium, it is interesting to note that the data between 1.0 and 1.5 GPa yield a slope of about 1.3 GPa.

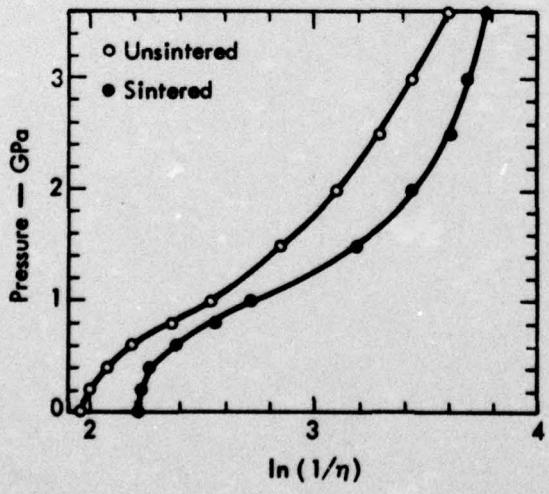

Fig. 16. Pressure as a function of ln $(1/\eta)$ for porous beryllium from the data in Figs. 1 and 2. Values for slope are at point indicated.

The very steep slopes in Figs. 15 and 16 indicate the need for a more complex form than Eq. (1) to fit the data. For example, the use of about 1.4 GPa as "a" in Eq. (1) will result in predicted pressures being over an order of magnitude too high. The data in Fig. 15 indicate yield at very low stress and, in order to obtain the appropriate slope, the coefficient a will have to be initially small but expand with decreasing η. If a is related to the yield of the material, this implies work hardening, and an effect of this type has been invoked by Holt et al.[13] to match experimental data on porous aluminum. However, in the case of beryllium, the amount of work hardening necessary to fit the data in Fig. 15 is far beyond that observed for polycrystalline or single crystal beryllium.[14,15] In the case of the unsintered material, we would need to increase the yield strength by over 100, when the equivalent plastic strain in the solid matrix is about 1, to be consistent with Eq. (1). Rather, we feel that such effects as variable pore size distribution, aspherical pores, and anisotropic crystal orientation in the matrix must play a large role.

If we consider a material containing a distribution of pore shapes and sizes as in Figs. 12(a) and 13(a), then we might expect significant departures from models

based on the collapse of a single spherical pore. First, there would be a range of yield stresses over which pores would collapse, with the more aspherical pores collapsing first. Second, larger pores would tend to collapse at lower stresses than smaller pores, if we make the assumption that the larger the pore the thinner the average pore wall. Both adjustments would be expected to modify these models in such a way as to yield relationships similar to those observed in Figs. 15 and 16. In addition to the photomicrographic evidence, we have seen in the unloading moduli evidence consistent with highly aspherical pores and large variations in pore size distribution. In this way, the effective strengths of successively more spherical and/or smaller pores are progressively being exceeded.

Conclusions

The data presented here allow several conclusions to be drawn concerning the physical response of porous beryllium to stress. Initial quasi-static yielding is seen to be much more pronounced in the sintered than in the unsintered material with the result that higher stresses are attained on initial loading in the sintered beryllium. This may simply be the result of the formation of more spherical and hence stronger pores in the sintering process or a reflection of decreased porosity in the sintered material, or both. On the other hand, it may represent the effect of residual stresses in the unsintered material such as outlined by Stevens and Pope[16] who envisaged these stresses lowering the applied shear stress necessary to cause yielding. Sintering presumably relieves residual stresses caused by cooling of the anisotropic beryllium grains.

We believe that the apparent lack of a strain-rate effect in the compaction of unsintered beryllium is because the effect is too small to be observed. A process that involves the movement of material into void space and therefore requires a finite time will exhibit inertial effects. It is reasonable to suppose that with more spherical pores (as in the sintered beryllium) that will withstand higher pressures and involve more displacement of material, a larger strain-rate effect will be observed.

The data in Figs. 5 and 8 indicate loading below the hydrostat under conditions of uniaxial strain. This could be related to the observed anisotropy (Figs. 9 and 10). In all cases the maximum applied stress was oriented normal to the isotropic plane. Thus at a given mean pressure, the stress normal to highly asymmetric pores lying in this plane is greater if the stress is uniaxial, rather than hydrostatic. Apparent corroboration for this hypothesis comes from observation of more pronounced anisotropy, and hence, greater enhanced compaction in the unsintered material than in the sintered material.

However there is another, and likely more effective, mechanism to explain the enhanced compaction in uniaxial strain. The presence of a macroscopic shear stress under conditions of uniaxial strain will cause a given pore to yield at a lower

mean pressure, than when the macroscopic stress field is hydrostatic, and give rise to shear-enhanced compaction, observed previously in porous earth materials.[17] This phenomenon is not taken into account in constitutive models[12,18] which do not treat the shear stress as contributing independently to the mean stress. At the higher strain rates associated with shock-loading, this effect may be less pronounced. Nevertheless it will be important in describing the collapse of porous materials at lower mean stresses when the shear stress is still an appreciable percentage of the mean stress. However, before constitutive relations can be confidently suggested, more experimental data than presented here must be obtained and over a wider variety of stress paths. The observed unstable pore collapse will tend to complicate this task somewhat.

The observation that at the maximum attained pressures of 4.0 GPa there is significant porosity remaining is somewhat perplexing. On the one hand it is consistent with a sizable amount of highly spherical, small pores. Support for this suggestion comes from the data in Fig. 11 and photomicrographic evidence of the material pressurized to 4.0 GPa. However, any reasonable estimate of the yield strength necessary to keep pores open at 4.0 GPa exceeds measured values for beryllium.[14,15] Furthermore the maximum attainable shear stresses in uniaxial strain (Figs. 3 and 6) are in very good agreement with the values obtained on solid nonporous polycrystalline beryllium.[14] Thus we are forced to the conclusion that we are dealing with one or more of 1) significant amounts of strong impurities such as BeO, 2) porosity so small as to involve microscopic and hence stronger than normal pores, or 3) a highly anisotropic aggregate of crystals arranged so as to take advantage of the strength of single crystal beryllium in its strongest direction (~2 GPa).[14] None of the material studied here showed more than 0.7 wt% of BeO on chemical analysis.[3]

In summary, we have shown that porous beryllium exhibits pore-collapse in a noncatastrophic fashion. However, this collapse does not appear to be easily described as suggested by some models and apparently verified with porous aluminum.[19] The difficulty with beryllium may lie in its anisotropic crystal structure with attendant anisotropic mechanical properties. In addition, the flame-spraying process induces significant anisotropy in the porosity, and presumably also in crystal orientation. These factors, in addition to pore size distribution and pore shape, could easily produce deviations from a simple model for a hollow sphere in an isotropic medium.

Acknowledgments

We thank J. Hanafee for supplying the photomicrographs in advance of publication and for helpful interpretations of them. We are indebted to H. C. Heard, W. Isbell, A. Holt, and H. Weed for critical review of the manuscript.

References

1. D. R. Stephens, J. Geophys. Res. 69, 2967 (1964).
2. R. N. Schock, H. C. Heard, and D. R. Stephens, J. Geophys. Res. 78, 5922 (1973).
3. W. Isbell and R. Horning, Behavior of Porous Beryllium under Thermo-Mechanical Loading, Part 3: Shock Wave Studies, Lawrence Livermore Laboratory, Rept. UCRL-51682 Pt. 3 (1974).
4. P. W. Bridgman, Proc. Am. Acad. Sci. 76, 55 (1948); ibid. 76, 71 (1948).
5. J. Hanafee and E. O. Snell, Behavior of Porous Beryllium under Thermo-Mechanical Loading, Part 6: Effect of Pressure on the Microstructure of Plasma-Sprayed Beryllium, Lawrence Livermore Laboratory, Rept. UCRL-51682 Pt. 6 (1974).
6. American Institute of Physics Hand Book (McGraw-Hill, New York, 1963), 2nd ed., p. 3-88.
7. J. K. Mackensie, Proc. Phys. Soc. London B 63, 2 (1950).
8. Z. Hashin, in Proc. IUTAM Symposium: Non-Homogeneity, Elasticity, and Plasticity, Warsaw (Pergamon Press, 1959), No. 17, pp. 463-478; J. Appl. Mecn. 29, 143 (1962).
9. J. B. Walsh, W. F. Brace, and A. W. England, J. Amer. Ceramic Soc. 48, 605 (1965).
10. R. W. Heckel, Trans. Met. Soc. AIME 221, 1001 (1961).
11. K. Konopicky: See R. Kieffer and W. Hotop, Sintereisen und Sinteristable (Springer-Verlag, Wien, 1948).
12. M. M. Carroll and A. C. Holt, J. Appl. Phys. 43, 1626 (1972).
13. A. C. Holt, M. M. Carroll, and B. M. Butcher, "Pore Structure and Property of Materials," in Proc. RILEM/IUPAL Symp., Prague, 1973.
14. N. Inoue, V. Damiano, J. Hanafee, and H Conrad, Trans. Met. Soc. AIME 242, 2081 (1968).
15. V. V. Damiano, J. E. Hanafee, G. J. London, and N. Inoue, Trans. Met. Soc. AIME 245, 637 (1969).
16. A. L Stevens and L. E. Pope, in Metallurgical Effects at High Strain Rates, R. W. Rhode et al., Eds. (Plenum, New York, 1973), pp. 459-472.
17. R. N. Schock, H. C. Heard, and D. R. Stephens, J. Geophys. Res. 78, 5922-5941 (1973).
18. W. Herrmann, J. Appl. Phys. 40, 2490 (1969).
19. R. N. Schock, A. E. Abey, and A. Duba, Trans. Amer. Geophys. Union 55, 420 (1974).

RERUN - 3/12/75
R. N. Schock (200)

RAC/lc/lm